



Prostaglandin E2 receptor EP1 (PGE₂/EP₁) deletion promotes glomerular podocyte and endothelial cell injury in hypertensive TTRhRen mice

Rania Nasrallah¹ · Joseph Zimpelmann¹ · Susan J. Robertson² · Jamie Ghossein¹ · Jean-Francois Thibodeau³ · C. R. J. Kennedy^{1,4} · Alex Gutsol⁴ · Fengxia Xiao⁴ · Dylan Burger^{1,4} · Kevin D. Burns^{1,4} · Richard L. Hébert¹

Received: 19 June 2019 / Revised: 5 August 2019 / Accepted: 20 August 2019 / Published online: 16 September 2019

© United States & Canadian Academy of Pathology 2019

Abstract

Prostaglandin E2 receptor EP1 (PGE₂/EP₁) promotes diabetic renal injury, and EP₁ receptor deletion improves hyperfiltration, albuminuria, and fibrosis. The role of EP₁ receptors in hypertensive kidney disease (HKD) remains controversial. We examined the contribution of EP₁ receptors to HKD. EP₁ null (EP₁^{-/-}) mice were bred with hypertensive TTRhRen mice (Htn) to evaluate kidney function and injury at 24 weeks. EP₁ deletion had no effect on elevation of systolic blood pressure in Htn mice (HtnEP₁^{-/-}) but resulted in pronounced albuminuria and reduced FITC-inulin clearance, compared with Htn or wild-type (WT) mice. Ultrastructural injury to podocytes and glomerular endothelium was prominent in HtnEP₁^{-/-} mice; including widened subendothelial space, subendothelial lucent zones and focal lifting of endothelium from basement membrane, with focal subendothelial cell debris. Cortex COX2 mRNA was increased by EP₁ deletion. Glomerular EP₃ mRNA was reduced by EP₁ deletion, and EP₄ by Htn and EP₁ deletion. In WT mice, PGE₂ increased chloride reabsorption via EP₁ in isolated perfused thick ascending limb (TAL), but PGE₂ or EP₁ deletion did not affect vasopressin-mediated chloride reabsorption. In WT and Htn mouse inner medullary collecting duct (IMCD), PGE₂ inhibited vasopressin-water transport, but not in EP₁^{-/-} or HtnEP₁^{-/-} mice. Overall, EP₁ mediated TAL and IMCD transport in response to PGE₂ is unaltered in Htn, and EP₁ is protective in HKD.

Introduction

Hypertension and diabetes are major causes of cardiovascular morbidity and mortality worldwide [1–3], and leading causes of chronic kidney disease, including hypertensive kidney disease (HKD) and diabetic kidney disease (DKD). Prostaglandin E₂ (PGE₂), the main renal product of cyclooxygenase 2 (COX2), stimulates renin secretion, and

regulates glomerular hemodynamics and tubular transport of salt and water, thereby contributing to blood pressure (BP) control [4, 5]. Inhibition of the PGE₂ synthesis enzymes, cyclooxygenase (COX), and microsomal PGE₂ synthase (mPGES1), causes hypertension [6–9]; but the contribution of PGE₂ to HKD remains unclear.

Renal effects of PGE₂ are mediated by four G protein coupled receptors, EP_{1–4}. Both COX2 and PGE₂ are elevated in diabetes [4, 10–16] and EP₁ is upregulated in diabetic glomeruli and proximal tubules promoting renal injury [17]. Antagonizing or knocking out EP₁ prevents diabetic hyperfiltration, kidney growth, and albuminuria [17, 18], suggesting that EP₁ could be targeted to improve renal outcomes in DKD.

EP₁ antagonism reduces BP in hypertensive type II diabetic db/db mice [19]. However, in the stroke prone spontaneously hypertensive rat, a model of malignant hypertension, EP₁ antagonism for 5 weeks reduced renal injury markers despite persistent hypertension [20]. Also, in a triple model of nephrectomized-deoxycorticosterone acetate (DOCA) salt-angiotensin II hypertension, EP₁ deletion improved renal outcomes, but BP was also lowered

✉ Richard L. Hébert
rlhebert@uottawa.ca

¹ Department of Cellular and Molecular Medicine, Faculty of Medicine, Kidney Research Centre, University of Ottawa, 451 Smyth Road, Room 2514, Ottawa, ON, Canada

² Department of Pathology and Laboratory Medicine, Ottawa, ON, Canada

³ Prometic Biosciences Inc., Kidney Research Centre, Laval, QC, Canada

⁴ Ottawa Hospital Research Institute, Kidney Research Centre, University of Ottawa, Ottawa, ON, Canada

[21]. We recently showed that EP₁ deletion does not reduce BP in young renin overexpressing TTRhRen hypertensive mice [22]. We also recently demonstrated that PGE₂/EP₁ inhibits water and sodium reabsorption in the mouse inner medullary collecting duct (IMCD) and cortical collecting duct (CCD) [22]. Since the BP lowering effect of EP₁ disruption is inconsistent, we sought to examine how PGE₂ affects thick ascending limb (TAL) and IMCD transport, to gain insight into the transport properties of the distal nephron in HKD, and the contribution of PGE₂/EP₁ receptors to renal injury and transport.

To gain mechanistic insight into the consequence of EP₁ deletion in HKD versus DKD, we bred EP₁ null mice with TTRhRen hypertensive mice, and measured markers of renal function and injury. We report that hypertensive mice lacking EP₁ have increased albuminuria and reduced GFR compared with wild-type hypertensive mice, but persistent hypertension, suggesting that renal EP₁ protects against HKD via BP-independent mechanisms.

Materials and methods

Mouse models

All animal procedures were approved by the University of Ottawa Animal Care Committee. Mice were housed on a 12-h light–dark cycle, with free access to standard chow and water. Male mice were studied at 24 weeks of age. The contribution of EP₁ was studied using FVB/n mice with gene-targeted EP₁ deletion (EP₁^{-/-} mice). These mice were generated and characterized at the Kidney Research Centre [23]. Hyperreninemic hypertensive TTRhRen [24, 25] transgenic mice (Htn) on the same FVB/n background were bred with EP₁^{-/-} to generate hypertensive mice lacking EP₁ (HtnEP₁^{-/-}). We examined the effect of EP₁ deletion on hypertensive mice at 24 weeks. Mice were randomly assigned to four groups: wild type (WT), EP₁^{-/-}, Htn, and HtnEP₁^{-/-}.

Blood pressure, metabolic cages, and urine analysis

Systolic blood pressure (SBP) was measured at the same time daily by tail-cuff plethysmography (BP 2000, Visitech systems, NC, USA). Following a 5-day training period, the average SBP of 5 consecutive days was calculated as previously done [22, 26]. Mice were placed in metabolic cages with free access to water and food. Twenty-four hours of food consumption, urine output, and water intake were recorded following a 24-h adaptation period. Urine osmolality was determined by freezing point depression (Advanced Model 3MO Plus Osmometer, Advanced Instruments Inc, MA, USA). Twenty-four hours of urine albumin was quantified by Mouse Albumin ELISA (Bethyl Labs, TX, USA) and

arginine vasopressin (AVP) excretion rates were measured using Arg⁸-Vasopressin ELISA (Enzo Life Sciences, NY, USA) and corrected for 24-h urine output.

Glomerular filtration rate (GFR)

GFR was estimated in conscious mice prior to kill by fluorescein isothiocyanate (FITC)-inulin clearance. Briefly, 5% of FITC-inulin (Sigma-Aldrich, St. Louis, MO, USA) dissolved in 0.9% saline was dialyzed overnight and filtered. Mice were injected with 3.74 μl/gBW of FITC-inulin via tail vein. Blood was collected from the saphenous vein into heparinized capillary tubes at seven intervals: 3, 7, 10, 15, 35, 55, and 75 min, and centrifuged. Samples were buffered in HEPES (500 mM, pH 7.4) and fluorescence was measured (excitation 488 nm/emission 538 nm). GFR was calculated using a two-compartment clearance model as previously reported [22, 26].

Quantitative PCR analysis

The left kidneys were dissected to separate cortex and medulla, and snap frozen in liquid nitrogen. Glomeruli were separated from cortex as previously reported by our group [27], and 50 glomeruli per mouse were used to isolate RNA. Briefly the cortex was minced and digested in 10 ml of perfusion solution containing 10 mg collagenase type IV (Sigma, St. Louis, MO, USA) gassed with a 95% O₂ to 5% CO₂ mixture at 37 °C. The digested mixture was serially sieved: 250, 105, and 75 μm. Individual glomeruli were isolated under the light microscope from the 75 μm suspension. Snap frozen tissue was homogenized using the TP-103 Amalgator COE Capmixer (GC America Inc, IL, USA). The RNAqueous Mini Kit (Invitrogen, MA, USA) was used to extract RNA from glomeruli and tissue RNA was isolated with TRIzol (Invitrogen, MA, USA) and treated with DNase I (Invitrogen, MA, USA). mRNA was measured by quantitative PCR (qPCR) with the ABI Prism 7000 system using specific primers as described, and the SYBR Advantage qPCR Premix (Clontech Laboratories, CA, USA) according to the manufacturer's instructions. The expression of COX2, EP₁, EP₃, and EP₄ was examined. Expression was normalized to 18S RNA and the 2(-Delta-DeltaC(T)) method was used for analysis as done previously [22]. Table 1 lists the primers used for qPCR.

Urine microparticle analysis

Urinary microparticles were assessed from 24-h urine samples by flow cytometry as described previously with modification [28, 29]. Briefly, urine samples were thawed rapidly and centrifuged at 2500 × g for 10 min at 4 °C to remove any large debris. Supernatants were then transferred

Table 1 Primer sequences for qPCR

Product name	Forward	Reverse
18S	5'-ATGGTAGTCGCCGTGCCTAC-3'	5'-CCGGAATCGAACCCCTGATT-3'
EP1 receptor	5'-AGTGCCAAGGGTGGTCCAA-3'	5'-CCGGGAACCTACGCAGTGAAC-3'
EP3 receptor	5'-GCCGCTATTGATAATGATGTTGAA-3'	5'-CCTTCTCCTTCCCATCTGTGT-3'
EP4 receptor	5'-ATGGTCATCTTACTCATCGCCAC-3'	5'-CTTTCACCACGTTTGGCTGAT-3'
COX2	5'-CAAGGGAGTCTGGAACATTG-3'	5'-ACCCAGTCTCGCTTATGA-3'

to a fresh tube and centrifuged for 20 min at $20,000 \times g$ at 4°C . The resultant supernatant was discarded and the microparticle pellet was re-suspended in filtered Annexin V binding buffer (10 mM HEPES, pH 7.4, 140 mM NaCl, 2.5 mM CaCl_2). Microparticles were labeled with a FITC-conjugated Annexin V (1:50 dilution, Biolegend, San Diego, CA, USA), and a Phycoerythrin (PE)-conjugated antipodoplanin antibody (1:100 dilution, Biolegend, San Diego, CA, USA) for 1 h. A PE-conjugated isotype IgG and Annexin V in buffer lacking calcium were employed as negative controls. Samples were analyzed on a Beckman Coulter Cytoflex at the University of Ottawa Flow Cytometry Core Facility.

Histology and electron microscopy

Mice were euthanized at 24 weeks of age. Histopathological analysis was performed in a blinded manner, on paraffin embedded sections, $4\ \mu\text{m}$ thick. The glomerular area (GA) was manually traced as the area within the outer capillary loops of the tuft in 12–18 glomeruli per mouse ($\times 63$ magnification). The mean glomerular volume (GV) was calculated from the measured GA as follows: $\text{GV} = (\text{GA})^{3/2} \times \beta/d$, where β is a dimensionless shape coefficient ($\beta = 1.38$ for spheres) and $d = 1.01$ is a size distribution coefficient that is used to adjust for variation in the glomerular size [30]. The capillary volume was measured as the volume of CD31-positive cells in the glomerulus. The capillary area (CA) stained positive to CD31 was quantified in 12–18 randomly selected glomeruli ($\times 63$ magnification). The capillary volume (CV) was calculated as follows: $\text{CV} = (\text{GV} \times \text{CA})/\text{GA}$. The results were averaged for each animal. Microscopy was performed with a Zeiss AX10 microscope (Oberkochen, Germany). Images were analyzed with ImagePro Plus software (Media Cybernetics, Bethesda, MD, USA).

Ultrastructural analysis of the glomerular filtration barrier was assessed in the four hypertensive groups by electron microscopy (three mice per group) as previously described [11]. Briefly, kidney cortex (0.5 mm cubes) were fixed in 2.5% (w/v) glutaraldehyde in phosphate buffered saline, placed into a Leica EM Tissue Processor, rinsed in cacodylate buffer, 2 h post fixation in 2% (w/v) osmium tetroxide, dehydrated through graded ethanols

and acetone, and infiltrated in three changes of Spurr's resin for 24 h. Blocks were cured at 65°C , sectioned ($80\ \mu\text{m}$) using a Leica Ultracut R ultramicrotome, stained with uranyl acetate/lead citrate, and screened on a Hitachi 7600 TEM. Images were captured using AMT digital camera software. Glomerular basement membranes (GBMs) were measured on images at $\times 30,000$ in zones with perpendicularly oriented foot processes. Between 30 and 140 measurements/mouse were made. At a magnification of $\times 10,000$ the GBM length was measured live with these images saved including the labeled measurement line. The peripheral open loops of entire glomeruli were sampled. Manual counting of foot processes along these measured lengths of GBM was done on the digital images. The slit pore diaphragm diameters were measured at $\times 60,000$ in regions with perpendicularly oriented foot processes.

In vitro microperfusion studies in IMCD and mTAL

Mice were euthanized at 24 weeks of age, and IMCD were microdissected for in vitro microperfusions and measurement of net fluid reabsorption (J_v).

^3H -inulin ($75\ \mu\text{Ci}/\text{ml}$) was used as a volume marker. In control periods, two collections were made for calculation of basal J_v following 30 min equilibration. Tubules with a negative basal J_v were discarded. AVP (10^{-12} mM, Sigma-Aldrich, St. Louis, MO, USA) was added to the bath and four 10-min collections were made. PGE_2 (10^{-7} mM, Sigma-Aldrich, St. Louis, MO, USA) was then added with five additional 10-min collections. Mean J_v was calculated as previously described [22, 26].

For measurement of mTAL chloride flux, mTAL were microdissected and chloride transport was studied in the absence of stimulation (baseline transport). The effect of PGE_2 on vasopressin-dependent chloride transport was studied with 10^{-6} mM PGE_2 stimulations following 10^{-7} mM AVP, which has been shown to stimulate TAL chloride transport [31]. Then experiments were repeated with PGE_2 stimulations first, followed by PGE_2 and AVP. Three collections were made for each period. Chloride concentrations were measured by microfluorometry (SPQ (6-Methoxy-N-(3Sulfopropyl) Quinolinium, Inner Salt); Molecular Probes, Eugene, OR, USA).

Characterization of hypertensive-diabetic mice lacking EP₁

Another subset of the four mouse groups were rendered diabetic with streptozotocin toxin (STZ) injection at 6–8 weeks of age, namely: wild-type diabetic (STZ), EP₁ null diabetic (STZEP₁), hypertensive diabetic (STZHtn), and EP₁ null hypertensive diabetic (STZHtnEP₁). Diabetes was induced with five-daily intraperitoneal injections of 50 mg/kg BW STZ (Sigma-Aldrich, St. Louis, MO). As a vehicle control, four mice from each nondiabetic group received Na citrate injections and were pooled with uninjected nondiabetic mice since no differences were observed in all the parameters measured. Diabetes induction was confirmed by blood glucose monitoring with a glucometer at 12 weeks of age. At 22 weeks of age, glucose was measured following a 16 h fast using a colorimetric assay as per the manufacturer's instructions (Glucose colorimetric assay Kit, Cayman Chemical, item no. 10009582).

Periodic acid–Schiff (PAS) staining and histopathological analyses were performed on diabetic mice. Glomerulosclerosis and tubulopathy was estimated on PAS-stained paraffin embedded sections, 4 μm thick, in a blinded manner. Renal lesions were quantified using a conventional semi-quantitative scoring approach [29] with minor modifications. Glomerulopathy was assessed according to the extent of mesangial cell proliferation, hyalinosis, and sclerosis. The glomerular injury score (GIS) was graded 0–3+, in which 0 was no injury, 1+ was injury up to 25% of the glomerulus, 2+ was 50%, and 3+ was injury of more than 50%. The GIS was calculated as the mean of scores assigned to 30 glomeruli in each mouse. Tubulopathy was assessed for tubular dilation, accumulation of PAS-positive droplets and atrophy of tubular epithelium. Tubular lesions

were graded from 0 to 3+, according to the severity of tubular dilations, in at least ten microscopic fields in each section.

For immunohistochemistry, antigen retrieval was done with TRIS/EDTA buffer pH 9.0. Glomerular capillaries were identified by platelet endothelial cell adhesion molecule-1 (CD31) with rabbit anti-CD31 antibody (Invitrogen, Carlsbad, CA, USA), dilution 1:100. Visualization was performed with ImmPRESS kits (Vector Lab, Burlingame, CA, USA) and 3-3'-diaminobenzidine tetrahydrochloride.

Statistics

Graphpad Prism (San Diego, CA, USA) was used for data analysis. Values are expressed as means ± SEM. Statistical analysis was done using parametric and nonparametric tests. One-way ANOVA followed by Tukey's post test and an unpaired *t*-test was performed for all experiments. The significance was indicated in results section for $p < 0.05$ by ANOVA. For EM analyses we also performed Kruskal–Wallis test followed by Dunn's multiple comparison test, and Mann–Whitney test. In addition, a one sample *t*-test with a hypothetical value of 1 was performed for qPCR.

Results

EP₁ deletion reduces glomerular filtration independent of blood pressure or volume status in hypertensive mice

To study the effect of chronic hypertension (24 weeks) and EP₁ receptor deletion on renal function, we measured glomerular filtration rate, kidney weights, volume status, and urine output. Body and kidney weights were unaltered in all

Table 2 Mouse parameters were measured at 24 weeks of age in four mouse groups: wild type (WT), EP₁ null (EP₁^{-/-}), hypertensive TTRhRen (Htn), and hypertensive EP₁ null (HtnEP₁^{-/-})

	WT	EP ₁ ^{-/-}	Htn	HtnEP ₁ ^{-/-}
Final body weight (BW, g)	29.5 ± 1.0	29.8 ± 1.0	30.2 ± 0.7	29.0 ± 0.5
Kidney weight (KW, g)	199.2 ± 8.8	204.2 ± 4.9	219.7 ± 9.5	205.9 ± 5.4
KW/BW (×10 ³)	6.2 ± 0.2	6.4 ± 0.2	6.5 ± 0.1	6.7 ± 0.1
Tibia length (TL, mm)	18.0 ± 0.3	18.2 ± 0.3	18.0 ± 0.1	18.1 ± 0.2
KW/TL (g/mm)	11.1 ± 0.5	11.1 ± 0.2	11.1 ± 0.3	11.3 ± 0.3
Food intake (g/day)	3.6 ± 0.1	3.6 ± 0.2	3.5 ± 0.2	3.8 ± 0.1
Water intake (ml/day)	3.1 ± 0.2	3.8 ± 0.2	3.8 ± 0.2	4.8 ± 0.3
Urine Volume (ml/day)	0.70 ± 0.05	0.74 ± 0.08	1.14 ± 0.07	1.78 ± 0.16
Urine Osmolality (×10 ³ mOsm/kg H ₂ O)	3.95 ± 0.25	3.58 ± 0.15	2.71 ± 0.17*	1.95 ± 0.10* ^{&%}
Urine Vasopressin (AVP; ×10 ³ pg/day)	1.01 ± 0.20	1.02 ± 0.14	1.61 ± 0.18*	1.53 ± 0.15*
Urine Albumin (×10 ³ μg/day)	8.2 ± 0.7	8.3 ± 1.5	354.6 ± 128.8	1494.0 ± 672.7

Data are presented as mean ± SEM, $n = 7–21$

* $p < 0.05$ vs WT; & $p < 0.05$ vs EP₁; % $p < 0.05$ vs Htn

hypertensive mice compared with WT, and kidney weights normalized to body weight or tibia length were also unchanged (Table 2). Food and water consumption were unchanged in $EP_1^{-/-}$, Htn, and Htn $EP_1^{-/-}$ compared with WT, but urine osmolality was significantly lower in Htn mice and Htn $EP_1^{-/-}$ mice compared with WT.

To examine whether EP_1 receptor deletion affected urinary AVP excretion, we measured AVP levels in urine collected for 24 h. AVP excretion rates were increased in Htn ($1.61 \pm 0.18 \times 10^3$ pg/day) and Htn $EP_1^{-/-}$ (1.53 ± 0.15) compared with WT mice (1.01 ± 0.20), and unaltered by EP_1 deletion (Table 2).

To examine whether EP_1 receptor deletion affected urinary albumin excretion, we measured albumin levels in urine collected for 24 h. As shown in Table 2, albuminuria was comparable in $EP_1^{-/-}$ (8.3 ± 1.5 μ g/day) and WT (8.2 ± 0.7 μ g/day) mice.

In Fig. 1, systolic BP was significantly higher in Htn (143.1 ± 2.8 mmHg) and Htn $EP_1^{-/-}$ (147.9 ± 3.3 mmHg) compared with WT (114.3 ± 2.7 mmHg). EP_1 deletion did not affect BP compared with WT. Glomerular filtration rate was unchanged in $EP_1^{-/-}$ (243.0 ± 31.1 μ l/min) and Htn mice (230.7 ± 28.1 μ l/min) compared with WT (245.8 ± 23.1 μ l/min), but significantly reduced in Htn $EP_1^{-/-}$ mice (164.5 ± 24.9 μ l/min).

Renal COX2, EP_1 , EP_3 , and EP_4 are altered in HKD

To study the effect of EP_1 deletion on expression of the renal COX2/PGE₂/EP receptor system in HKD and DKD, we performed qPCR analysis on renal cortex and medulla, as well as microdissected glomeruli. As shown in Fig. 2, the expression of cortical COX2 was unchanged in Htn mice (1.5 ± 0.3 -fold WT), but increased in mice lacking EP_1 , to 2.2 ± 0.1 -fold WT in $EP_1^{-/-}$, and 2.5 ± 0.6 -fold WT in Htn $EP_1^{-/-}$. Medullary COX2 expression was comparable in all groups (data not shown). In microdissected glomeruli, EP_1 expression was unchanged in Htn mice (data not shown). Similarly, EP_3 receptors were unchanged in Htn mice, but significantly reduced by 75% in mice lacking EP_1 receptors ($EP_1^{-/-}$ and Htn $EP_1^{-/-}$). EP_3 expression was also significantly lower in Htn $EP_1^{-/-}$ mice compared with Htn. Glomerular EP_4 receptors were reduced in all mouse groups up to 90% compared with WT.

EP_1 deletion alters urinary microparticle excretion in HKD

Microparticles are emerging biomarkers of cellular stress/injury. To study the effect of EP_1 deletion on urinary microparticle levels in HKD, we characterized the origin of

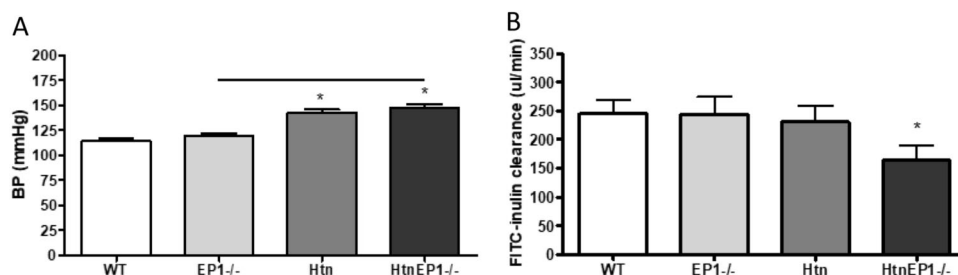


Fig. 1 Systolic blood pressure (BP, $n = 10$ – 21) and FITC-inulin clearance ($n = 7$ – 13) were measured in four mouse groups: wild type (WT), EP_1 null ($EP_1^{-/-}$), hypertensive TTRhRen (Htn), and

hypertensive EP_1 null (Htn $EP_1^{-/-}$). Data are presented as mean \pm SEM. $p < 0.05$ * vs WT. Line indicates significance between groups

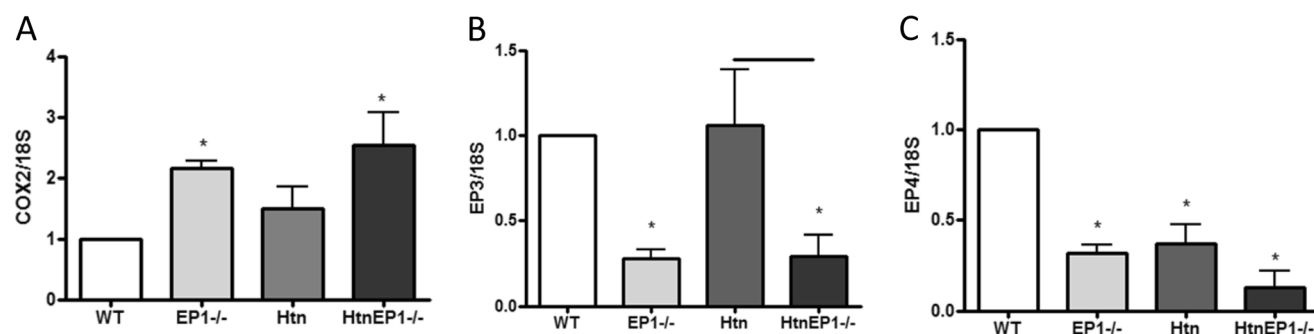


Fig. 2 Quantitative PCR analysis of COX2 in the cortex (a, $n = 5$ – 9) was performed in four mouse groups at 24 weeks of age: wild type (WT), EP_1 null ($EP_1^{-/-}$), hypertensive TTRhRen (Htn), and hypertensive EP_1 null (Htn $EP_1^{-/-}$). EP_3 (b) and EP_4 (c) receptors were

measured in microdissected glomeruli ($n = 5$ – 6). Data were normalized to 18S and presented as fold change of mean \pm SEM. $*p < 0.05$ vs WT, black line indicates significance between groups

the urine microparticles by flow cytometry using podoplanin (podocyte-derived) and annexin V labeling (all sources). Total Annexin V-labeled microparticles were not significantly different in all groups compared with WT mice ($4.6 \pm 1.2 \times 10^9$ /mg creatinine), however there was ~65% less urinary microparticles from HtnEP₁^{-/-} ($2.2 \pm 0.4 \times 10^9$ /mg creatinine) compared with EP₁^{-/-} ($6.3 \pm 1.1 \times 10^9$ /mg creatinine) mice ($P = 0.004$). Similarly, podoplanin positive microparticles were not significantly different between all groups compared with wild-type mice, but again levels were reduced in HtnEP₁^{-/-} ($7.8 \pm 1.4 \times 10^7$ /mg creatinine) compared with EP₁^{-/-} ($2.0 \pm 0.5 \times 10^8$ /mg creatinine) mice ($P = 0.03$).

EP₁ deletion promotes injury in HKD

PAS-stained sections were scored for glomerular and tubular injury. Glomerular injury was undetectable in WT, EP₁^{-/-}, and Htn mice, and negligible in HtnEP₁^{-/-} mice (data not shown). Therefore, to assess ultrastructural injury, we performed electron microscopy analyses of the glomerulus and filtration barrier of hypertensive mice. As shown in Fig. 3a–c, ultrastructural injury to podocytes and glomerular endothelium was prominent in HtnEP₁^{-/-} compared with WT mice, with podocyte vacuolation and foot process widening. The endothelium was lifted from the

GBM, and the subendothelial space was widened with electron-lucent fluffy material and focal cell debris. Overall there were no morphological anomalies in WT or EP₁^{-/-} mice. Two Htn mice showed short run or patchy foot process fusion and one mouse showed focal podocyte vacuoles, but all three Htn mice showed microvesicle blebs. Average foot processes lengths are shown in Fig. 3d, with increased length in EP₁^{-/-} mice from 302.2 ± 12.5 nm in WT to 431.1 ± 15.4 nm, although this did not reach statistical significance. As shown in Fig. 3e, the GBM thickness was significantly reduced in EP₁^{-/-} mice from 188.1 ± 6.9 nm in WT mice to 164.7 ± 3.0 nm. However, GBM thickness was significantly elevated in HtnEP₁^{-/-} mice (215.2 ± 10.5) compared with EP₁^{-/-} and Htn mice. Finally, in Fig. 3f, slit pore diameters are increased in mice lacking EP₁, from 0.030 ± 0.001 μ m in WT to 0.041 ± 0.001 and 0.041 ± 0.002 in EP₁^{-/-} and HtnEP₁^{-/-}, respectively.

PGE₂/EP₁ stimulates water and chloride transport in IMCD and mTAL

The main site of renal EP₁ expression is in the collecting duct (CD), where PGE₂/EP₁ activation promotes diuresis and natriuresis. We measured fluid reabsorption (J_v) in the IMCD and chloride flux in the mTAL, in response to PGE₂

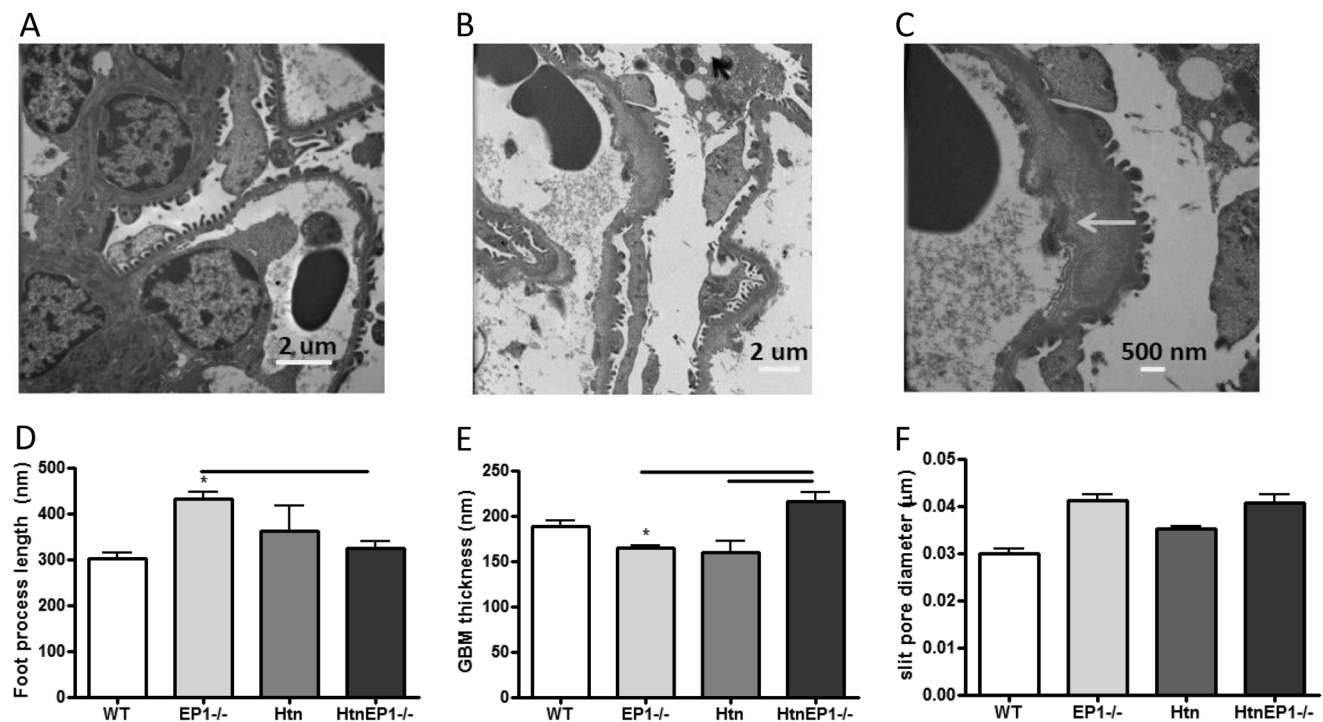


Fig. 3 Electron microscopy analysis at 24 weeks in four mouse groups: wild type (WT), EP₁ null (EP₁^{-/-}), hypertensive TTRhRen (Htn), and hypertensive EP₁ null (HtnEP₁^{-/-}). **a** Representative micrograph of wild-type control at 10,000 \times ; **b** Representative micrograph of HtnEP₁^{-/-} mouse at 8000 \times showing podocyte vacuolation (red arrow) and foot process widening (blue arrow); **c** same image as B showing

endothelial degeneration, lifting from glomerular basement membrane, and subendothelial insudate at 17,000 \times (green arrow). Average **d** foot process length ($n = 3$); **e** glomerular basement membrane thickness ($n = 3$); and **f** slit pore diameters ($n = 2-3$) are shown as mean \pm SEM. * $p < 0.05$ vs WT, and black line indicates significance between groups

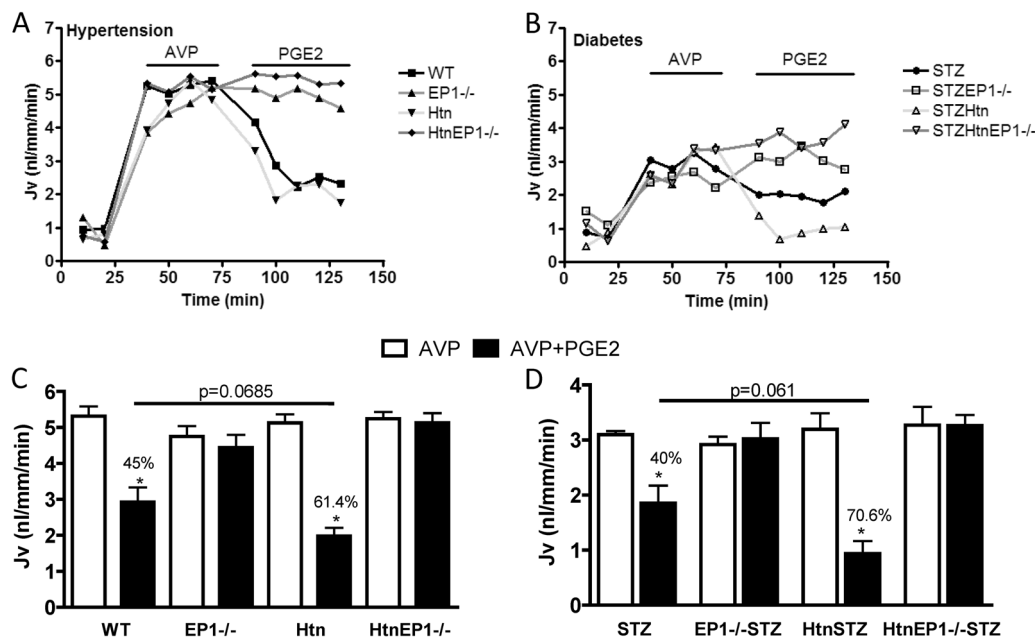


Fig. 4 Net fluid reabsorption (J_v) was analyzed in eight mouse groups with hypertension (HTn) and/or streptozotocin (STZ) diabetes: wild type (WT and STZ), EP1 null (EP1^{-/-} and STZEP1^{-/-}), hypertensive TTRhRen (Htn and STZHtn), and hypertensive EP1 null (HtnEP1^{-/-} and STZHtnEP1^{-/-}). The terminal inner medullary collecting ducts were microdissected for in vitro microperfusion and determination of J_v (nl/mm/min). A representative time course in minute (min) of J_v is shown for hypertension (a) and diabetes (b), the stimulation period in

absence (AVP) and presence of PGE₂ is indicated with black line above the tracings. Bar graphs are shown for hypertension (c) and diabetes (d) of mean \pm SEM, $n = 3-9$. Tubules were stimulated with 10^{-12} M vasopressin (AVP: white bars) and AVP with 10^{-7} M PGE₂: black bars). Asterisk symbol indicates significance versus AVP, $p < 0.05$, and black line indicates significance between two groups with respective p -value

stimulation in the presence or absence of AVP. PGE₂ inhibits AVP-mediated fluid reabsorption in microdissected terminal IMCD. A representative tracing of J_v over time is shown for one IMCD from each group (Fig. 4). As shown in Fig. 4c, AVP increased J_v to 5.3 ± 0.3 nl/mm/min in WT IMCD, but the AVP response was comparable in the other nondiabetic groups. PGE₂ significantly attenuated AVP-mediated J_v by 45% in WT (2.9 ± 0.4) and 61.4% in Htn mice (2.0 ± 0.2) compared with AVP alone, but not in EP1^{-/-} (4.4 ± 0.4) or HtnEP1^{-/-} (5.1 ± 0.3) mice. In STZ mice shown in Fig. 4d, AVP-stimulated J_v was 42% lower than WT mice only reaching 3.1 ± 0.1 nl/mm/min. Again, the AVP response was comparable in all diabetic groups. PGE₂ also attenuated AVP-mediated J_v by 40 and 70.6% in STZ (1.9 ± 0.3) and STZHtn (0.9 ± 0.2) mice respectively, but not in mice lacking EP1.

We examined whether the transport properties of the TAL are altered in long-standing HKD, and whether PGE₂/EP1 is involved in TAL chloride transport. As shown in Fig. 5, AVP significantly increased chloride transport, from 67.1 ± 8.8 pmol/mm/min to 163.9 ± 17.1 in WT mice. There was no difference in the magnitude of the AVP response in the four groups, and PGE₂ and EP1 deletion had no effect on AVP-mediated chloride reabsorption. In a second set of experiments, when PGE₂ was added prior to AVP stimulation, PGE₂ significantly

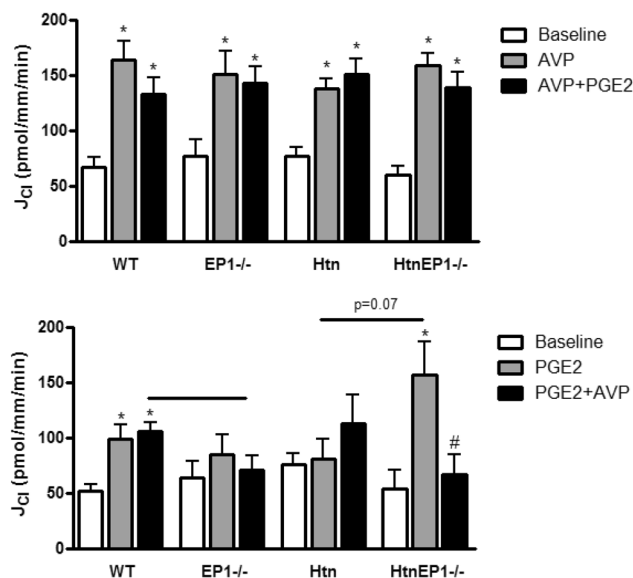


Fig. 5 Chloride reabsorption (J_{Cl}) was analyzed in four mouse groups: wild type (WT), EP1 null (EP1^{-/-}), hypertensive TTRhRen (Htn), and hypertensive EP1 null (HtnEP1^{-/-}). The medullary thick ascending limb were microdissected for in vitro microperfusion and determination of J_{Cl} (pmol/mm/min). The upper graph shown chloride reabsorption in response to 10^{-6} M vasopressin (AVP) then 10^{-6} M PGE₂ in the presence of AVP ($n = 4-6$). In the lower graph PGE₂ was added first followed by AVP in the presence of PGE₂ ($n = 4$). Data are shown as mean \pm SEM. * $p < 0.05$ vs baseline, # $p < 0.05$ vs PGE₂, and black line $p < 0.05$ between two groups or respective p -value

increased chloride reabsorption from 51.4 ± 5.9 to 98.9 ± 12.9 pmol/mm/min in WT mice. As shown, when AVP was added to WT mice following PGE₂ stimulations, the magnitude of the AVP response was lower than the first set of experiments, and chloride reabsorption was only increased twofold by AVP, reaching 105.9 ± 8.2 pmol/mm/min. The baseline chloride transport did not differ between groups, and the response to PGE₂ was also similar. EP₁ deletion attenuated AVP-stimulated chloride reabsorption following PGE₂ stimulation from 105.9 ± 8.2 in WT mice to 71.1 ± 12.1 and 66.9 ± 17.8 in EP₁^{-/-} and HtnEP₁^{-/-} mice, respectively. The AVP response post-PGE₂ was comparable in Htn (112.2 ± 26.4) and WT (105.9 ± 8.2) mice. However, in HtnEP₁^{-/-} mice, PGE₂-mediated chloride transport was increased to 156.3 ± 30.2 compared with 98.9 ± 12.9 in WT mice, and there was a significant 50% attenuation of chloride transport upon co-stimulation with PGE₂ + AVP (66.9 ± 17.8) compared with PGE₂ alone (112.2 ± 26.4).

EP₁ deletion is protective in DKD

To compare the effect of EP₁ deletion in the nondiabetic state with diabetes, we analyzed certain renal parameters in mice rendered diabetic by streptozotocin (STZ) injection (shown in Table 3) and compared them with renal parameters of nondiabetic mice shown in Table 2. As shown in Table 3, diabetic hyperglycemia was not affected by EP₁ deletion or hypertension, but all diabetic mice were hyperglycemic compared with nondiabetic WT mice levels of 6.40 ± 1.02 mg/dL.

Body weights were reduced, and kidney weights were increased in all diabetic mice. As shown in Table 3, EP₁ deletion did not affect kidney to body or kidney to tibia length ratios in diabetic mice, but kidney to tibia length ratio was significantly lower in STZHtnEP₁^{-/-} compared with STZ mice, from 16.4 ± 0.6 to 13.3 ± 0.8 . Diabetic mice consumed about twofold more chow than nondiabetics. Food intake was significantly lower in STZEP₁^{-/-} and STZHtnEP₁^{-/-} mice compared with STZ mice. In diabetic mice water intake was up to tenfold higher than nondiabetics, but EP₁ deletion significantly reduced water intake in STZEP₁^{-/-} and STZHtnEP₁^{-/-} compared with STZ mice.

Urine volume was increased almost 50-fold in STZ mice compared with WT, but significantly reduced in STZEP₁^{-/-} mice. This reduction was reversed in STZHtnEP₁^{-/-} mice. In all diabetic mice, urine osmolalities were reduced compared with nondiabetics, but also STZHtn and STZHtnEP₁^{-/-} osmolalities were significantly lower than their respective controls (Htn and HtnEP₁^{-/-}).

AVP excretion rates were increased in STZ mice 20-fold, but significantly reduced in STZEP₁^{-/-} (10.84 ± 2.80), STZHtn (13.57 ± 3.22), and STZHtnEP₁^{-/-} (12.70 ± 2.16) compared with STZ mice (21.63 ± 3.70). AVP excretion rates in diabetic mice were all also significantly higher than their respective controls. Albumin was significantly increased in STZHtn mice (19180 ± 5501) compared with WT and STZ mice. In diabetic mice, BP was increased to 134.7 ± 4.4 mmHg and slightly more in STZHtn mice (151.4 ± 3.8) but was not significantly different than STZ alone. STZ mice were hyperfiltering to 551.8 ± 28.1

Table 3 Mouse parameters were measured at 24 weeks of age in four mouse groups with streptozotocin (STZ) diabetes: wild type (STZ), EP1 null (STZEP₁^{-/-}), hypertensive TTRhRen (STZHtn), and hypertensive EP₁ null (STZHtnEP₁^{-/-})

	STZ	STZEP ₁ ^{-/-}	STZHtn	STZHtnEP ₁ ^{-/-}
Fasting blood glucose (mg/dL)	31.14 ± 0.81	30.82 ± 0.48	26.70 ± 1.70	29.00 ± 1.40
Final body weight (BW, g)	26.0 ± 0.6	25.0 ± 0.9	26.0 ± 0.6	24.3 ± 0.7
Kidney weight (KW, g)	304.2 ± 9.4	261.9 ± 16.6	279.7 ± 58.1	$238.7 \pm 14.8^{\#}$
KW/BW ($\times 10^3$)	10.3 ± 0.2	$8.9 \pm 0.6^{\#}$	10.6 ± 0.2	9.4 ± 0.3
Tibia length (TL, mm)	18.6 ± 0.2	18.1 ± 0.2	18.4 ± 0.2	18.0 ± 0.2
KW/TL (g/mm)	16.4 ± 0.6	14.5 ± 0.9	15.0 ± 0.8	$13.3 \pm 0.8^{\#}$
Food intake (g/day)	8.4 ± 0.2	$6.3 \pm 0.6^{\#}$	7.9 ± 0.5	$7.0 \pm 0.4^{\#}$
Water intake (ml/day)	40.9 ± 1.5	$23.1 \pm 4.6^{\#}$	34.0 ± 3.4	$34.2 \pm 3.1^{\#, \$}$
Urine Volume (ml/day)	33.38 ± 1.22	$18.31 \pm 4.40^{\#}$	28.21 ± 3.25	$29.44 \pm 2.63^{\$}$
Urine Osmolality ($\times 10^3$ mOsm/kg H ₂ O)	1.03 ± 0.02	1.20 ± 0.12	1.06 ± 0.06	0.99 ± 0.03
Urine Vasopressin (AVP; $\times 10^3$ pg/day)	21.63 ± 3.70	$10.84 \pm 2.80^{\#}$	$13.57 \pm 3.22^{\#}$	$12.70 \pm 2.16^{\#}$
Urine Albumin ($\times 10^3$ μ g/day)	75.4 ± 33.4	4.72 ± 1.5	$19180.0 \pm 5501.0^{\#}$	10315.0 ± 3177.0
FITC-inulin clearance (μ l/min)	551.8 ± 28.1	385.4 ± 53.6	381.9 ± 45.3	302.4 ± 33.5
Systolic blood pressure (mmHg)	134.7 ± 4.4	125.0 ± 3.2	151.4 ± 3.8	144.3 ± 6.3

Data are presented as mean \pm SEM, $n = 3-9$

[#] $p < 0.05$ vs STZ; ^{\$} $p < 0.05$ vs STZEP₁^{-/-}

compared with WT, but GFR was significantly lowered in STZEP₁^{-/-} (385.4 ± 53.6), STZHtn (381.9 ± 45.3) and STZHtnEP₁^{-/-} (302.4 ± 33.5) compared with STZ alone.

In Fig. 6 injury in diabetic mice was quite prominent unlike nondiabetic mice (data not shown). In STZ mice, very mild glomerular injury was observed with an average score of 0.9 ± 0.2. The score was comparable in STZEP₁^{-/-} mice (0.9 ± 0.2). In STZHtn mice, the mean injury score was significantly increased to 1.7 ± 0.5. Finally, in the STZHtnEP₁^{-/-} mice, glomerular injury was significantly increased up to 2.3 ± 0.5. Tubule dilatation and injury were also scored from 0–3+. A mild score was observed in WT mice (0.2 ± 0.1), EP₁^{-/-} mice (0.3 ± 0.2), Htn mice (0.4 ± 0.2), and HtnEP₁^{-/-} mice (0.6 ± 0.2). In Fig. 6, tubule dilatation and injury are shown for diabetic mice. All 8 STZ mice (1.9 ± 0.2) showed signs of injury, and even greater in STZHtn (2.5 ± 0.3) and STZHtnEP₁^{-/-} (2.2 ± 0.3) mice. The injury was slightly lower in STZEP₁^{-/-} mice (1.4 ± 0.4) compared with STZ, but the difference was not significant. There was no significant difference by ANOVA in overall injury scores between diabetic groups.

CD31 labeling was used to examine CV. Mean CV was 52107 ± 10036 μm³ in WT mice, and unchanged in all nondiabetic groups (data not shown). As shown in Fig. 7, CV was elevated in STZ (108702 ± 6117) and STZHtn (96922 ± 10998) mice compared with WT. STZEP₁^{-/-} mice (70093 ± 5883) had significantly reduced CVs compared with STZ mice, but STZHtn and STZHtnEP₁^{-/-} volumes were no different than STZ. GVs were also measured and followed the same pattern of change as CVs in the different groups.

Discussion

The contribution of PGE₂/EP₁ to HKD is unclear. We previously showed that EP₁ deletion improves hyperfiltration, albuminuria, and fibrosis in several diabetic models [17]. The purpose of this study was to examine the contribution of PGE₂/EP₁ to long-standing HKD in mice, in comparison with hypertensive diabetic mice. We present novel data indicating that hypertensive mice (Htn) lacking EP₁ receptors (HtnEP₁^{-/-}) have worsened renal outcomes despite moderate sustained hypertension also seen in Htn mice. In this regard, EP₁ deletion increases albuminuria and reduces GFR in HtnEP₁^{-/-} mice, with prominent injury to podocytes and glomerular endothelium, but the mechanism is unclear. Two major conclusions from this work are that PGE₂/EP₁ is protective in HKD, and this effect is independent of BP.

The role of renal PGE₂/EP₁ in BP regulation is multifaceted. EP₁ deletion does not impair sodium excretion in the healthy kidney; however, EP₁^{-/-} mice display elevated renin and aldosterone levels consistent with sustained activation of the renin-angiotensin system [32], and an impaired pressor response to angiotensin II [33]. EP₁^{-/-} DBA/1lacJ mice had lower BP than EP₁^{+/+} mice, and a 0.02% salt diet lowered BP even further [32]. And in a triple model of nephrectomized-DOCA salt-angiotensin II hypertension, EP₁ deletion attenuated the rise in BP and promoted survival [21]. However, in our model of long-standing moderate hypertension, EP₁ deletion did not alter systolic BP, and volume status was maintained in both hypertensive and diabetic-hypertensive mice. Despite this, EP₁ deletion worsened albuminuria and reduced GFR in hypertensive

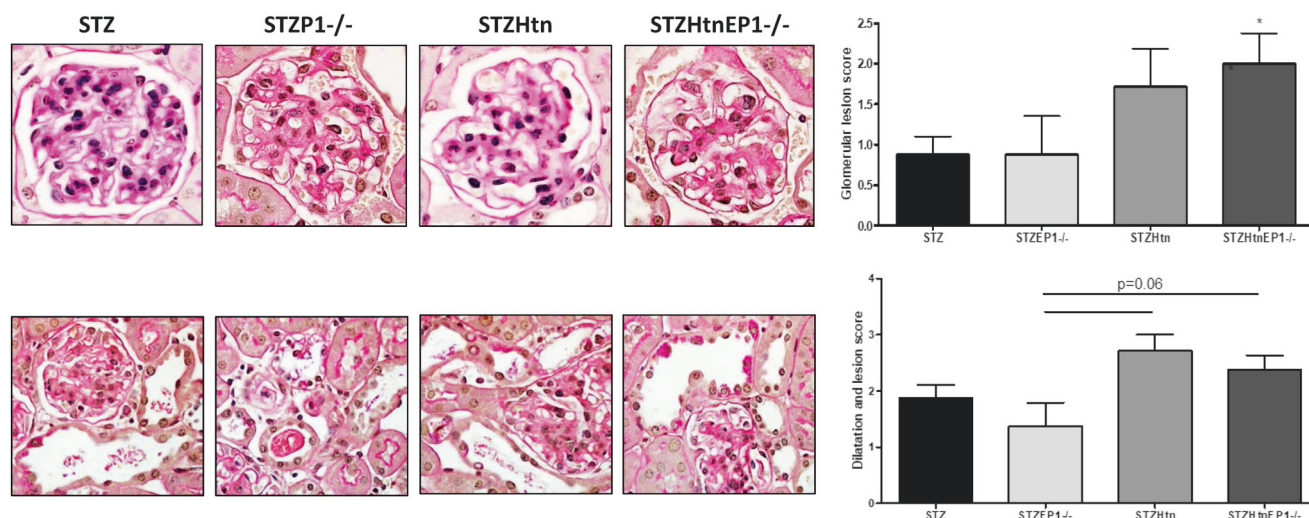


Fig. 6 Representative images for glomerular lesions (**top**) and tubular dilation/lesions (**bottom**) were scored on PAS-stained sections (×63) and (×40), respectively, taken at 24 weeks of age from four mouse groups with streptozotocin (STZ) diabetes: wild type (STZ), EP₁ null (STZEP₁^{-/-}), hypertensive TTRhRen (STZHtn), and hypertensive EP₁

null (STZHtnEP₁^{-/-}). lesions were scored blinded from 0–3+. Data are presented as mean ± SEM. **p* < 0.05 vs WT. Data are presented as mean ± SEM. **p* < 0.05 vs STZ. Line indicates statistical significance between two groups

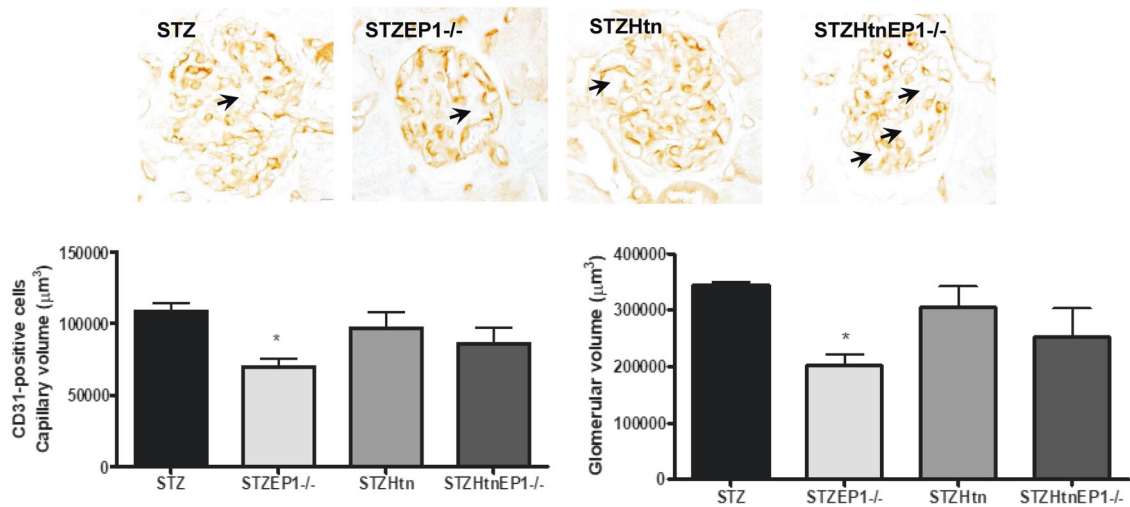


Fig. 7 Representative images of CD31 in glomeruli at 24 weeks of age from four mouse groups with streptozotocin (STZ) diabetes: wild type (STZ), EP₁ null (STZEP₁^{-/-}), hypertensive TTRhRen (STZHtn), and hypertensive EP₁ null (STZEP₁^{-/-}). Zones with absence of CD31 are

indicated with arrowheads. Capillary volume was estimated from CD31-positive cells and glomerular volumes were measured. Data were shown as mean ± SEM, *n* = 3–4. **p* < 0.05 vs STZ

mice. It is evident that EP₁ is needed to protect against endothelial and podocyte injury in hypertension, as revealed by the ultrastructural injury observed in mice lacking EP₁. Indeed, mice lacking EP₁ receptors exhibited significantly lower WT1 staining. Moreover, foot process lengths were reduced and GBM was thickened in HtnEP₁^{-/-} mice compared with EP₁^{-/-} mice. The mechanisms resulting in GBM thinning in EP₁^{-/-} and Htn mice require further clarification, as well as the role of EP₁ in foot process length. Interestingly, the HtnEP₁^{-/-} mice displayed lower levels of microparticles than the EP₁^{-/-} mice despite clear podocyte injury. Similar reductions were seen in Annexin V⁺ microparticles. The origin(s) of Annexin V⁺ microparticles in urine is unclear but they likely arise from a mixture of podocytes and various tubular epithelial cell subpopulations. While traditionally, high levels of microparticles are seen with tissue injury, it is possible that the reductions observed here are due to the advanced nature of the injury in HtnEP₁^{-/-} mice resulting in lower podocyte and tubular cell endowment.

The exact mechanisms were not fully explored in this study, but in the absence of EP₁, cortical COX2 is increased and glomerular EP₃ and EP₄ expression are reduced. Clearly, EP₁ may have a role to play in maintaining EP receptor expression, and the loss of these three receptors may have deleterious consequences to the glomerular filtration barrier. Of interest, EP₁ deletion did not affect the tubules in hypertensive mice, but in diabetic mice, both EP₁ deletion and superimposed hypertension caused similar degrees of tubular dilatation and injury. Despite these tubular effects, transport responses were mostly intact. While PGE₂ had no effect on vasopressin-stimulated chloride transport in the medullary TAL if

vasopressin was added first, in the absence of vasopressin PGE₂ caused a significant increase in TAL chloride reabsorption. Not only did PGE₂ attenuate the magnitude of the vasopressin response when added prior to vasopressin, EP₁ mediates this attenuation considering that deletion further reduced the magnitude of the AVP response. The role of specific PGE₂/EP receptors in TAL transport has not been thoroughly studied. Peterson et al. [34] demonstrated that PGE₂ inhibits chloride reabsorption in microperfused rat TAL segments, but the mechanism was not well characterized. Also, in addition to inhibiting AVP-dependent chloride reabsorption, PGE₂ attenuated AVP-dependent transepithelial voltage in isolated perfused mouse medullary TAL but had no effect on its own [35]. Again, the EP receptors involved, or transport mechanisms were not fully studied. However, PGE₂ was shown to inhibit medullary TAL sodium potassium 2 chloride (NKCC2) transport in cultured mouse TAL cells [36]. Though little is known about the PGE₂/EP pathways mediating TAL responses, we recently confirmed the expression of EP_{1, 3, 4} receptors in microdissected mouse TAL by qPCR [22]. It was also shown that PGE₂ induces chloride secretion in cultured mouse inner medullary and CCD cells in culture, but the role of CD EP receptors has not been fully characterized [37, 38].

We have recently shown that in mouse IMCD, PGE₂/EP₁ plays a key role in inhibiting AVP-dependent water reabsorption and determined that the inhibition of sodium transport by PGE₂/EP₁ in the CCD occurs via ENaC and pendrin-dependent pathways [22]. Consistent with our previous work [22] PGE₂ significantly attenuated AVP-mediated water reabsorption in the mouse IMCD following 24 weeks of hypertension, and this response was not seen in

mice lacking EP₁. Interestingly, the attenuation of AVP-mediated transport by PGE₂ was greater in Htn mice than WT mice, suggesting that the IMCD may be more sensitized to PGE₂ or more PGE₂/EP₁ receptors are present in Htn IMCD. Another noteworthy finding is that the magnitude of the AVP-mediated water reabsorption is lower in diabetic mice than nondiabetics, but this was not different in all diabetic groups. As in nondiabetic mice, EP₁ mediates the attenuation of AVP effects on water transport in response to PGE₂. Taken together, the data suggest that EP₁ receptors mediate TAL and IMCD transport responses to PGE₂, but the transport is unaltered in Htn; and EP₁ receptors play a protective role in HKD. The role of EP₁ seems to be disease dependent, hypertension versus diabetes, but also the magnitude and duration of hypertension are clearly important as well. Further studies are needed to better understand how in acute malignant hypertension EP₁ causes injury, and in moderate long-standing hypertension EP₁ is protective. There are several possible explanations, including differences in the contribution of other EP receptors, other prostaglandins, or other hormonal systems that are differentially involved depending on the various models. But future comparisons of these models should help elucidate key differences in pathomechanisms of kidney injury, to offer better therapeutic intervention strategies.

Compliance with ethical standards

Conflict of interest The authors declare that they have no conflict of interest.

Publisher's note Springer Nature remains neutral with regard to jurisdictional claims in published maps and institutional affiliations.

References

- Lim SS, Vos T, Flaxman AD, Danaei G, Shibuya K, Adair-Rohani H, et al. A comparative risk assessment of burden of disease and injury attributable to 67 risk factors and risk factor clusters in 21 regions, 1990–2010: a systematic analysis for the Global Burden of Disease Study 2010. *Lancet*. 2012;380:2224–60.
- Olsen MH, Angell SY, Asma S, Boutouyrie P, Burger D, Chirinos JA, et al. A call to action and a lifecourse strategy to address the global burden of raised blood pressure on current and future generations: The Lancet Commission on hypertension. *Lancet*. 2016;388:2665–712.
- Harcourt BE, Penfold SA, Forbes JM. Coming full circle in diabetes mellitus: from complications to initiation. *Nat Rev Endocrinol*. 2013;9:113–23.
- Nasrallah R, Hassouneh R, Hébert RL. Chronic kidney disease: Targeting prostaglandin E2 receptors. *Am J Physiol Renal Physiol*. 2014;307:F243–50.
- Swan CE, Breyer RM. Prostaglandin E2 modulation of blood pressure homeostasis: studies in rodent models. *Prostaglandins Other Lipid Mediat*. 2011;96:10–3.
- Gurwitz JH, Avorn J, Bohn RL, Glynn RJ, Monane M, Mogun H. Initiation of antihypertensive treatment during nonsteroidal anti-inflammatory drug therapy. *JAMA*. 1994;272:781–6.
- Yang T. Microsomal prostaglandin E synthase-1 and blood pressure regulation. *Kidney Int*. 2007;72:274–8.
- Whelton A, White WB, Bello AE, Puma JA, Fort JG. Effects of celecoxib and rofecoxib on blood pressure and edema in patients or 65 years of age with systemic hypertension and osteoarthritis. *Am J Cardiol*. 2002;90:959–63.
- White WB, Kent J, Taylor A, Verburg KM, Lefkowitz JB, Whelton A. Effects of celecoxib on ambulatory blood pressure in hypertensive patients on ACE inhibitors. *Hypertension*. 2002;39:929–34.
- Nasrallah R, Hassouneh R, Hébert RL. Prostaglandin E2, kidney disease, and cardiovascular risk: beyond hypertension and diabetes. *J Am Soc Nephrol*. 2016;27:666–76.
- Nasrallah R, Robertson SJ, Karsh J, Hébert RL. Celecoxib modifies glomerular basement membrane, mesangial area and podocyte structure in OVE26 mice, but ibuprofen is more detrimental. *Clin Sci*. 2013;124:685–94.
- Nasrallah R, Robertson SJ, Hébert RL. Chronic COX inhibition reduces diabetes-induced hyperfiltration, proteinuria, and renal pathological markers in 36-week B6-Ins2(Akita) mice. *Am J Nephrol*. 2009;30:346–53.
- Nasrallah R, Xiong H, Hébert RL. Renal prostaglandin E2 receptor (EP) expression profile is altered in streptozotocin and B6-Ins2Akita type 1 diabetic mice. *Am J Physiol*. 2007;292:278–84.
- Cherney DZ, Miller JA, Scholey JW, Nasrallah R, Hébert RL, Dekker MG, et al. Renal hyperfiltration is a determinant of endothelial function responses to cyclooxygenase 2 inhibition in type 1 diabetes. *Diabetes Care*. 2010;33:1344–6.
- Cherney DZI, Miller J, Scholey JW, Bradley TJ, Slorach C, Curtis JR, et al. The effect of cyclooxygenase 2 inhibition on renal hemodynamic function in humans with type 1 diabetes mellitus. *Diabetes*. 2008;57:688–95.
- Cherney DZ, Scholey JW, Nasrallah R, Dekker MG, Slorach C, Bradley TJ, et al. Renal hemodynamic effect of cyclooxygenase 2 inhibition in young men and women with uncomplicated type 1 diabetes mellitus. *Am J Physiol Renal Physiol*. 2008;294:F1336–41.
- Thibodeau JF, Nasrallah R, Hébert RL, Kennedy C. Reduced albuminuria in diabetic PTGER1-null mice. *Am J Pathol*. 2013;183:1789–802.
- Makino H, Tanaka I, Mukoyama M, Sugawara A, Mori K, Muro S, et al. Prevention of diabetic nephropathy in rats by prostaglandin E receptor EP1-selective antagonist. *J Am Soc Nephrol*. 2002;13:1757–65.
- Rutkai I, Feher A, Erdei N, Henrion D, Papp Z, Edes I, et al. Activation of prostaglandin E2 EP1 receptor increases arteriolar tone and blood pressure in mice with type 2 diabetes. *Cardiovasc Res*. 2009;83:148–54.
- Suganami T, Mori K, Tanaka I, Mukoyama M, Sugawara A, Makino H, et al. Role of prostaglandin E receptor EP1 subtype in the development of renal injury in genetically hypertensive rats. *Hypertension*. 2003;42:1183–90.
- Bartlett CS, Boyd KL, Harris RC, Zent R, Breyer RM. EP1 disruption attenuates end-organ damage in a mouse model of hypertension. *Hypertension*. 2012;60:1184–91.
- Nasrallah R, Zimpelmann J, Eckert D, Ghossein J, Geddes S, Beique JC, et al. PGE2/EP1 receptor inhibits vasopressin-dependent water reabsorption and sodium transport in mouse collecting duct. *Lab Invest*. 2018;98:360–70.
- Kennedy CRJ, Xiong H, Rahal S, Vanderluit J, Slack R, Zhang Y, et al. Urine concentrating defect in prostaglandin EP1-deficient mice. *Am J Physiol*. 2007;292:F868–75.
- Araki K, Imaizumi T, Sekimoto T, Yoshinobu K, Yoshimuta J, Akizuki M, et al. Exchangeable gene trap using the Cre/mutated lox system. *Cell Mol Biol*. 1999;45:737–50.

25. Thibodeau JF, Holterman CE, Burger D, Read NC, Reudelhuber TL, Kennedy CR. A novel mouse model of advanced diabetic kidney disease. *PLoS One*. 2014;9:e113459.
26. Hassouneh R, Nasrallah R, Zimpelmann J, Gutsol A, Eckert D, Ghossein J, et al. PGE2 receptor EP3 inhibits water reabsorption and contributes to polyuria and kidney injury in a streptozotocin-induced mouse model of diabetes. *Diabetologia*. 2016;59:1318–28.
27. Wehbi GJ, Zimpelmann J, Carey RM, Levine DZ, Burns KD. Early streptozotocin-diabetes mellitus downregulates rat kidney AT2 receptors. *Am J Physiol Renal Physiol*. 2001;280:F254–65.
28. Burger D, Thibodeau JF, Holterman CE, Burns KD, Touyz RM, Kennedy CR. Urinary podocyte microparticles identify pre-albuminuric diabetic glomerular injury. *J Am Soc Nephrol*. 2014;25:1401–7.
29. Raj L, Azar S, Keane W. Mesangial immune injury, hypertension, and progressive glomerular damage in Dahl rats. *Kidney Int*. 1984;26:137–43.
30. Weibel ER. *Stereological Method: Practical Methods of Biological Morphometry*. Vol. 1. London: Academic Press; 1979.
31. Himmerkus N, Plain A, Marques RD, Sonntag SR, Paliege A, Leipziger J, et al. AVP dynamically increases paracellular Na⁺ permeability and transcellular NaCl transport in the medullary thick ascending limb of Henle's loop. *Pflugers Arch - Eur J Physiol*. 2017;469:149–58.
32. Stock JL, Shinjo K, Burkhardt J, Roach M, Taniguchi K, Ishikawa T, et al. The prostaglandin E2/EP1 receptor mediates pain perception and regulates blood pressure. *J Clin Invest*. 2001;107:325–31.
33. Guan Y, Zhang Y, Wu J, Qi Z, Yang G, Dou D, et al. Anti-hypertensive effects of selective prostaglandin E2 receptor subtype 1 targeting. *J Clin Invest*. 2007;117:2496–505.
34. Peterson LN, McKay AJ, Borzecki JS. Endogenous Prostaglandin E2 Mediates Inhibition of Rat Thick Ascending Limb Cl Reabsorption in Chronic Hypercalcemia. *J Clin Invest*. 1993;91:2399–407.
35. Culpepper RM, Andreoli TE. Interactions among Prostaglandin E2, Antidiuretic Hormone, and Cyclic Adenosine Monophosphate in Modulating Cl⁻ Absorption in Single Mouse Medullary Thick Ascending Limbs of Henle. *J Clin Invest*. 1983;71:1588–601.
36. Kaji DM, Chase HS Jr, Eng JP, Diaz J. Prostaglandin E2 inhibits Na-K-2Cl cotransport in medullary thick ascending limb cells. *Am J Physiol Cell Physiol*. 1996;271:C354–61.
37. Rajagopal M, Thomas SV, Kathpalia PP, Chen Y, Pao AC. Prostaglandin E2 induces chloride secretion through crosstalk between cAMP and calcium signaling in mouse inner medullary collecting duct cells. *Am J Physiol Cell Physiol*. 2014;306:C263–78.
38. Sandrasagra S, Cuffe JE, Regardsoe EL, Korbmacher C. PGE2 stimulates Cl⁻ secretion in murine M-1 cortical collecting duct cells in an autocrine manner. *Pflugers Arch*. 2004;448:411–21.